

# Smart control for the chaotic dynamics using two regions uniform fiber Bragg grating

ZAINAB RASHEED GHAYIB<sup>1,2,\*</sup>, AYSER A. HEMED<sup>1,\*</sup>

<sup>1</sup>Department of Physics, College of Education, Mustansiriyah University, Baghdad, Iraq

<sup>2</sup>Diyala directorate of education, Diyala, Iraq

Two Self Electro-Optic Effect Device (SEED) laser diode devices were used in a new configuration. With this optics component, the Fiber Bragg Grating (FBG) acts as a smart reflector/filter controller at 1550 nm Bragg wavelength. Temperature and stress variation are employed to control the injected signal specifications before its modulation into Laser Diode (LD2). Results showed that chaotic emission outside of the laser device cavity is a promising technique. The SEED effect has an extreme contribution for these effect. Low cross correlation 0.1088-0.52899 between these two lasers approves an anti-synchronization between them. This ensure and guaranties for none periodical repetition for the dynamics between them, and then enhancement of chaotic transmitter security level.

(Received December 12, 2021; accepted August 10, 2022)

*Keywords:* Anti-synchronization, Fiber Bragg grating, Self-electro optic device, Chaotic transmitter, Cross correlation

## 1. Introduction

Recently, the use of high frequency electro-optical modulation to create a tunable self-mixing chaotic laser is proposed. A laser dynamics system with two degrees of freedom is devised and tested for adjustable chaotic laser production and provides optical feedback and electro-optic modulation [1]. The contests of the amplified spontaneous emission, the injected signal, and their beatings often dictate the nonlinear dynamics of an external optical injection system. In one hand, instabilities such as periodic and chaotic behaviors can be induced by the injection signal [2] [3]. It can, on the other hand, be used to improve frequency stability, increase bandwidth, and minimize noise and distortion characteristics. The chaotic behavior of such systems has recently been brought forward for cryptography applications due to its unpredictability [4].

A substantial anisotropy exists between Transverse electric (TE) and transverse magnetic (TM) modes due to the hetero-structure of a standard edge-emitting laser. Unless induced strain or other band structure modification techniques are used, these devices usually emit in a single, well-defined polarization state [5]. In contrast, because there is no a priori polarization discrimination, the symmetric transverse structure of VCSELs may cause polarization instabilities [6] [7]. It demonstrates polarization dynamics that are unstable due to anisotropic structures in their laser materials that disrupt the circular transverse symmetry. Although they emit Linearly Polarized (LP) light at threshold, an increase in injection current or a change in temperature can cause them to convert to orthogonal linear polarization, a process known as Polarization Switching (PS); see Ref. [11]. These polarization changes were typically interpreted (switch between x-LP and y-LP modes) as the laser operating

conditions; thermal, noise induced, bias current processes were modified during the operating [8].

A chaotic behavior was unambiguously identified as the result of the polarization mode competition [7]. Worth to mention, polarization beating between x and y electromagnetic wave components needs to be included in case of transmitting a signal with no polarization maintaining fibers [9]. A widely tunable microwave frequency far beyond the laser's Relaxation Oscillation (RO) frequency is observable with optical injection due to all optical structures. However, phase noise induced by the SLs' spontaneous emission noise is intrinsically included in this dynamics, which could extend the microwave line width and limit the practical applications of microwave signals [10]. With this operation, rate equations model for the free running laser diode should be include new terms. In case of optical communications, modulation adds new considerations for these equations. According to Ref [11], an external feedback element is added to a single SL equation in complex form under steady-state circumstances, resulting in the field equation for a complex cavity laser system.

In single type modulation, the injection current  $I(t)$  is made up of three components: a bias component  $I_b$ , a sinusoidal component of wave amplitude  $I_m$ , and the modulation frequency  $\nu_m$  [11];

$$I(t) = I_b + I_m \sin(2\pi\nu_m t) \quad (1)$$

A proper examination includes the connection of the laser diode to an external optical system, as well as the treatment of open cavities, or cavities with a low quality factor. Even for a single laser diode cavity, the common method of defining basic modes with equal mirror losses uniformly distributed along the cavity underestimates the

relationship between spontaneous-emission noise inside the laser mode. As a result, a complete picture for modeling laser dynamics under Optical Feedback (OFB) must include an operator that fully describes feedback effects, and then apply this technique to various suggested feedback geometries, such as variation in the diode internal cavity optical path length  $LD$ , which is caused by active medium crystal refractive index variation due to active region instantaneous temperature change with time [11].

Techniques for optical injection in laser diode recently estimated with the aid of fiber Bragg grating, FBG, with

which, light portion that satisfy Bragg wavelength can be reinjected into the laser device and a remaining portion transmitters. Fiber sensors are innovative sensors that have advanced rapidly in recent decades [12]. By monitoring the reflection and transmission spectra of FBG, we may acquire temperature and strain change values. The grating period, or fiber core refractive index  $n_{eff}$ , will change as the ambient temperature, strain, or other physical quantities change, and the reflection spectrum and transmission spectrum of FBG will change as well, causing the center wavelength of the fiber grating to shift, as shown in Fig. 1.

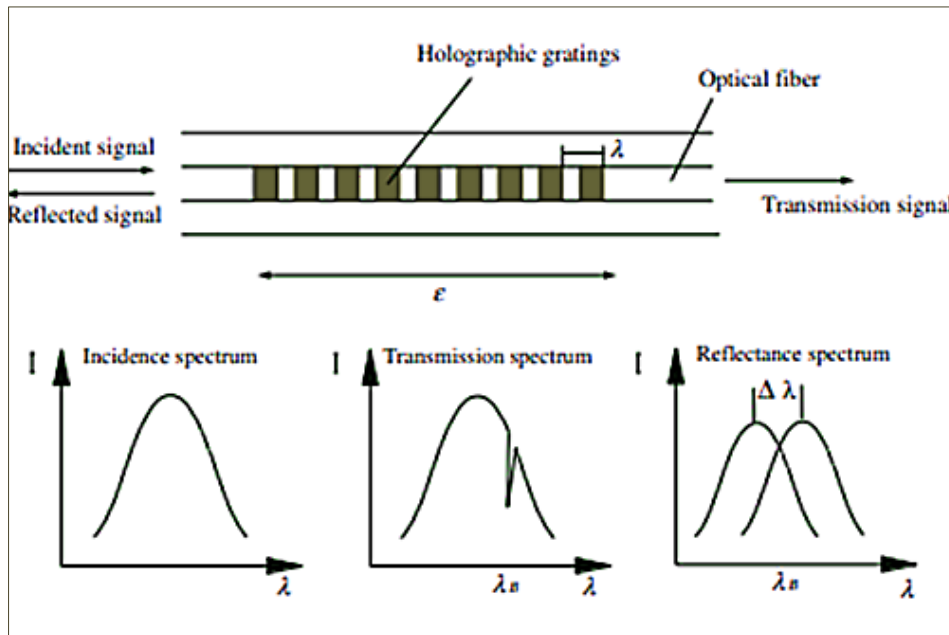


Fig. 1. Schematic diagram of FBG sensing principle

A guided mode propagating in uniform FBG can be coupled to another propagating in the opposite direction to generate a narrow-band reflection, and the peak reflection wavelength  $\lambda_B$  can be expressed as [13];

$$\lambda_B = 2n_{eff}\Lambda \quad (2)$$

When  $\lambda_B$  is the Bragg wavelength,  $n_{eff}$  is the fiber transmission mode's effective refractive index, and  $\Lambda$  is the grating pitch. By differential transformation with regard to Eq. (2), we may obtain the wavelength shift of FBG,  $\Delta\lambda_B$ , which is produced by strain and temperature difference  $\Delta T$ ;

$$\frac{\Delta\lambda_B}{\lambda_B} = (\alpha_f + \xi)\Delta T + (1 - P_e) \quad (3)$$

where,  $\alpha_f$ ,  $\xi$  and  $P_e$  are thermal expansion coefficient, thermo-optical coefficient and elasto-optical coefficient of fiber optic materials [13].

The basic idea behind FBG sensing is to track the peak position of the FBG by measuring the reflected spectrum and assuming a linear relationship between the

observed peak position and a genuine physical property like strain or temperature [14] via elasto – optic effect [9]. The most popular and commercially available FBGs operate in the 1550 nm range since low-cost telecommunications equipment is available at that wavelength [14]. The wavelength selection is accomplished by filtering light of a certain wavelength from a light source, resulting in a low output intensity and so restricting the system's maximum detection distance. This property can be employed in a "smart selection" for light portions via reflector/filter optical part. This technique for wavelength tuning is used with optical fiber chaotic lasers. The majority of these technologies, however, rely on tunable fiber Bragg gratings (TFBGs), which have wavelength tuning ranges of a few nanometers. The maximum sensor number in a WDM-based FBG sensing system is mostly limited by the short tunable wavelength ranges of FBGs [15]. The application of Bragg wavelength to adapt reflected wavelength in sensors is dependent on longitudinal strain/vibration, fiber temperature, and pressure/vibration [16].

When exposed to external disturbances, LDs can display a range of complicated dynamics, including steady

state, period, period doubling, quasi-periodicity, and chaos. Optical chaos creation based on the simplest perturbation system, optical feedback, has received a lot of attention because of its potential uses in secure communications [17], fiber amplifiers [18], random number generation, and chaotic lidar/radar [19].

It's important to keep in mind that, while the relaxation oscillation frequency rises with injected power, the modulation bandwidth may be smaller than in the free-running case due to a frequency dip in the SL's modulation response [20]. A SEED is a promising component that can operate as an optical logic element in future optical information processors. SEED makes use of the Quantum-Confined Stark Effect (QCSE), which is induced by an electric field and results in a change in the optical absorbance of Multiple Quantum Well (MQW) devices [21].

The form of the photocarrier density rate equation as eq. (4) is [22];

$$\frac{dn}{dt} = -\frac{n}{\tau} + \frac{\alpha P_{in} \Omega_0}{\{\omega - \omega_0 + \beta(V_0 - \eta R n)\}^2 + (\frac{\Omega_0}{2})^2} \quad (4)$$

where R is the resistive load, n photocarrier density,  $P_{in}$  is the power of incident light,  $\Omega_0$  is the half width of the absorption spectrum corresponding to the inverse of the life time of excitons and  $\omega$  is the light frequency,  $\beta$  is a parameter representing the rate of spectral shift due to QCSE and  $\omega_0$  is the central peak frequency of the exciton absorption spectrum in the absence of externally applied electric fields across the insulator layer,  $\tau$  carrier relaxation time and  $\alpha$  is the rate of photocarrier generation brought from dissociated excitons generated by light absorption in the intrinsic region consisting of the quantum well. The stationary solution of eq. (4) gives "bistability" with regard to light power  $P_{in}$ , and the results match those given by Tokuda *et al.* [22].

When the optical carrier frequencies of an injected and injection laser are detuned to the order of the Relaxation Oscillation Frequency (ROF), chaotic fluctuation might develop. In this phase for chaos generation, the optical-carrier frequency of the detuning, as well as the strong coupling, are most likely to occur [16];

$$\frac{dA}{dt} = -\frac{\gamma_c}{2} A + i(w_0 - w_c)A + \frac{\Gamma}{2}(1 - ib)gA + F_{sp} + \eta A_i \exp(-i\Omega t) \quad (5)$$

$$\frac{dN}{dt} = \frac{J}{ed} - \gamma_s N - \frac{2\epsilon_0 n^2}{\hbar w_0} g |A|^2 \quad (6)$$

where  $\eta$  is the injection coupling rate,  $A_i$  is the amplitude of the field injection at an optical frequency  $\omega_i$  and  $\Omega = \omega_i - \omega_0$  is the detuning frequency of the optical injection. The equation of complex field given has to be use because of the phase difference  $\phi$ , between the injection field  $A_i$  and the intracavity oscillating field which is nonlinearly coupled to the magnitude of oscillating field and is not arbitrary. It is possible to reformulate this

equation in the form of two coupled real rate equations in terms of  $\phi$  and  $|A|$  [16].

Fiber birefringence is frequently linked to polarization effects in fiber-optic communication systems [9]. Standard single-mode fibers support two orthogonally polarized modes, as is well known [3]. These two modes have almost the same propagation constant, which means they travel at nearly the same speed [4]. When light encounters any form of disruption or asymmetry within the fiber, it results quite easy for optical energy to flow from one of these modes to the other. Such disturbances or asymmetries cause random polarization rotation, polarization-mode coupling, and polarization-mode dispersion in sufficiently long fibers [23].

In optical data transfer via fiber optics, good electro-optic and optoelectric interconnects are required. Each of these requirements has been approved with seed. These seed devices can be found in quantum well materials. These devices may operate at high speeds while consuming very little energy, and they require far less hardware than pure optical feedback [24] [25] and optoelectronic methods [16] [26].

Fiber Birefringence is usually linked to polarization effects in fiber-optic communication systems [23] [9]. Light State of Polarization (SOP) in fiber optics communication systems remains mostly hard to control. SOP of a light wave after traveling over a few hundred meters in a fiber due to residual birefringence or strain remains completely unexpected. Polarization attraction or polarization tugging describes this phenomenon: the nonlinear interaction of the signal SOP with a Continuous Wave (CW) polarized pump beam stabilized it. Polarization instabilities in optical fibers may emerge from combining the degree of freedom for polarization with nonlinearity. In the presence of chromatic dispersion, optical fiber polarization modulation instabilities can be exploited to shift the frequency of a pump laser to new wavelength regions and generate ultrashort Brilliant or dark pulse trains. First-class devices include the Brillouin, Raman, and parametric amplifiers. Because they are based on polarization selective gain, these devices do not preserve beam energy and, more significantly, have a high level of output Relative Intensity Noise (RIN). In reality, because only the parallel to the pump polarization component of the input signal is amplified, SOP variations in the input signal must necessarily translate into substantial output intensity fluctuations [27]. One of the unexplained factors in current commercial FBGs is the Polarization Dependence Frequency Shift (PDFS), which is generated by birefringence in the fiber/FBG and is also reliant on grating inscription process. FBG shape distortion and asymmetry, FBG Full Width at Half Maximum (FWHM) limit, Side Lobe Suppression Ratio (SLSR), reflectivity, coating type and uniformity, and other characteristics all have the potential to effect total device efficiency. The application and measurement time scale dictate the major performance characteristics in sensing applications [28].

Seed makes anti-synchronization possible, a phenomenon in which the slaved seed oscillator has the

same amplitude as the master oscillator but opposite signs. Anti-synchronization allows for the strengthening of chaotic 3D attractors with identical complexity in each low-correlated oscillator. If nonlinear dispersion occurs, signal transfers without modifying its temporal profile, which can compensate for material dispersion, according to Ref. [29]. With high enough optical powers, this effect can also affect the mixing dynamics between two laser signals. Signal filtering [30], sensors [31] and complex networks [32] (such as anti-synchronized oscillators) are used to define a variety of phenomena in nature and technology, from physics and neuroscience to engineering and socioeconomic systems [16].

## 2. Simulation setup

Fig. 2 depicts a light source, while Table 1 contains abbreviations for analysis visualizations. Two SEEDed laser diode devices were used in a new configuration, one was used as an injector Laser Diode, LD1, and the other, LD2, as a follower and then chaotic transmitter. Detected LD1 emission is directed toward LD2 bias current. This

signal, before its detection, suffers from variation in its both portion and polarization. The former is determined by reflected/transmitted contribution with two regions FBG temperature and stress sensor. The FBG two separated regions have slightly varying Bragg wavelengths to give it a more effective weight. LD1, with a wavelength of 1550 nm, generating a light signal that was previously manipulated electronically with a virtual noise source. To see free running dynamics and trace the signal during the experiment, light is split into two parts by a normal splitter, with part one directed toward a detection (with amplification) arm. Part two was sent through an optical isolator to provide LD1 isolation from its back reflected light. This portion strikes the smart FBG1 from the left, causing light with the same wavelength as its Bragg wavelength ( $\lambda_B = 1549$  nm) to be reflected (deflected) into the right and then passing via a polarization control (simulated with 20 and 45 degree). Otherwise, remaining wavelengths of  $\lambda_B \neq 1549$  nm pass through it, indicating the transmitted portion. This component is likewise divided into two pieces for trace reasons: detection and main portion, which is guided into a second smart

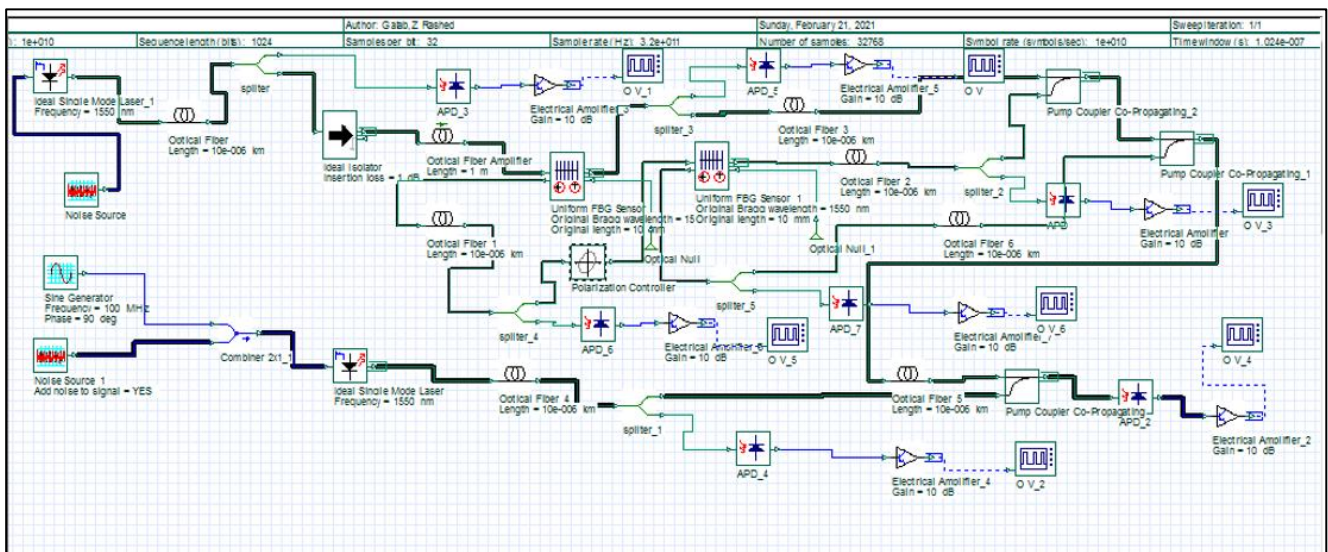


Fig. 2. Simulation set up (color online)

FBG2 with  $\lambda_B = 1550$  nm. By default, light which is satisfy this condition will have reflected back and going to pump coupler co-propagating\_1. While, transmitted part is directed to pump coupler co-propagating\_2, then pump coupler co-propagating\_1. All coupled portion is directed again to a third coupler, pump coupler co-propagating, in order to mix with light that came from another light source, LD2.

This laser has the same Characteristics of LD1 but modulated with another noise source with simulation values of (100, 200). LD2 itself is used to carry a frequency modulated message signal generated by FM modulator. Strain in both FBGs is simulated with values (250, 500, 1000) MPa.

Table 1. Abbreviations for simulation setup

Abbreviation	Meaning
O V	The time series of transmitted spectrum from FBG
O V_1	Oscilloscope visualizer for observe the time series LD spectrum
O V_2	Oscilloscope visualizer for observe the time series of LD_1 spectrum
O V_3	Oscilloscope visualizer for observe the time series of transmitted spectrum from FBG 1
O V_4	Oscilloscope visualizer for observe the time series after combiner between spectrum from pump coupler co-propagation-1.
APD	amplified photodetector for detect and observed radio frequency dynamics for reflected spectrum from FBG_1 before going inside the pump coupler co-propagation .
APD_1	amplified photodetector for detect and observe radio frequency dynamics for spectrum transmitted from FBG_1 before going inside the pump coupler co-propagationm-2.
APD_2	amplified photodetector for detect and observe radio frequency dynamics for spectrum transmitted from FBG before going inside the pump coupler co-propagation-2
APD_3	amplified photodetector for detect and observe radio frequency dynamics for LD1 before going inside the simulation circuit
APD_4	amplified photodetector for detect and observe radio frequency dynamics for LD 2 before going inside the simulation circuit

### 3. Results and discussion

Observations were made in order to trace the light step by step and accurately interprets the final results i.e. the signal detected in OV\_4. Part of these data can be analyzed directly via OptiSystem, while others, such as FFT (to detect laser frequency spectrum) and cross

correlations (to measure anti-synchronization), require the Origin program as well as Microsoft Excel. The effect of phase varied modulation into second laser output chaotic signal is verified in our earlier study; Ref. [16]. The polarization was kept constant in that investigation, and the FBG was simply has a one region. We've changed the affected parameters to include polarization rather than phase, and the FBG contains two regions instead of one. With specific control parameters including; stress, furthermore SEED in both LD1 and LD2.

#### 3.1. Injection with selected LD1 and LD2 SEED (constant FBG temperature and stress)

As shown in Fig. 2, in order to compare difference between emission for both LD1 and LD2, visualization was carried out for both devices by OV\_1 and OV\_2, respectively. Results for these observations are shown in Fig. 3, in which resulted time series between each measurement from these observations are not repeated in the remaining observations. This is due to the effect of SEED into these optoelectronic devices. SEED makes use of the Quantum-Confined Stark Effect (QCSE) [22]. Additionally, combination for this device LD1 with LD2 signal as a quantum well, causes changes in the active medium optical absorption. As a result, induced changes happens in an electric field that propagates perpendicularly to the quantum well material's for the thin semiconductor layers.

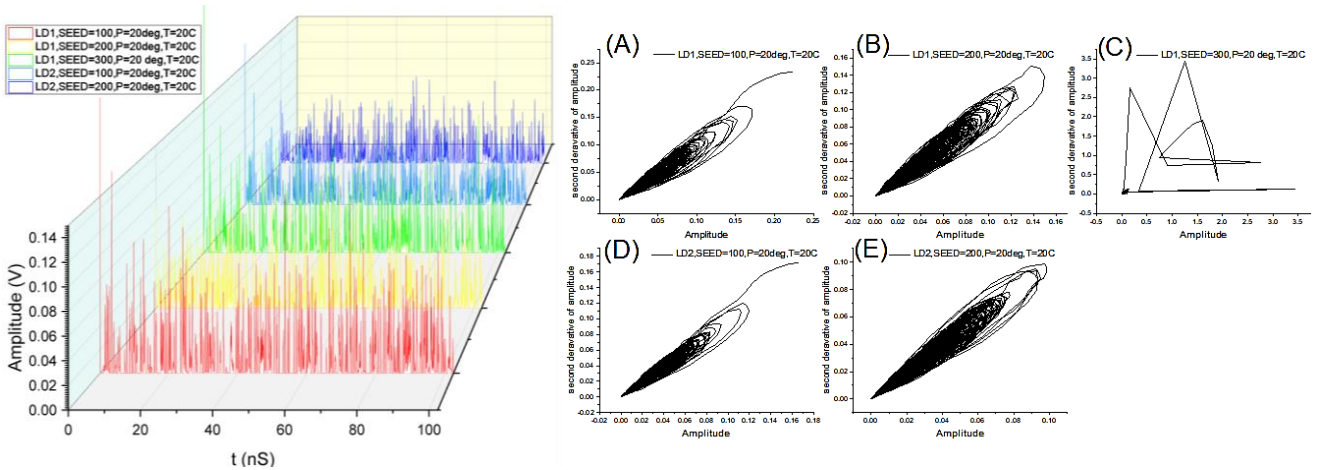


Fig. 3. Results for chaotic dynamics associated with LD1 (OV\_1) with variable seed (100, 200, 300), and LD2 (OV\_2) SEED (100, 200), with constant temperature  $T$  ( $20^{\circ}\text{C}$ ) and polarization  $P$  ( $20\text{ deg.}$ ). (left) Time series (right) Phase space. (A) LD1 SEED (100)  $P(20\text{ deg.})$ , (B) LD1 SEED (200)  $P(20\text{ deg.})$ , (C) LD1 SEED (300)  $P(20\text{ deg.})$ , (D) LD2 SEED (100)  $P(20\text{ deg.})$ , (E) LD2 SEED (200)  $P(20\text{ deg.})$  (color online)

The difference in emission between all observed time spectra is related with the nature of this effect, non-periodicals, that our goal is based on which for generating chaotic dynamics. Contribution for LD1 and LD2 SEEDs into resulted dynamics are shown also in part (b) from the

same figure. SEEDs values tested for three values (100, 200, 300), which represents randomness for oscillated modes. These attractors give the map of emission variation due to these changes.

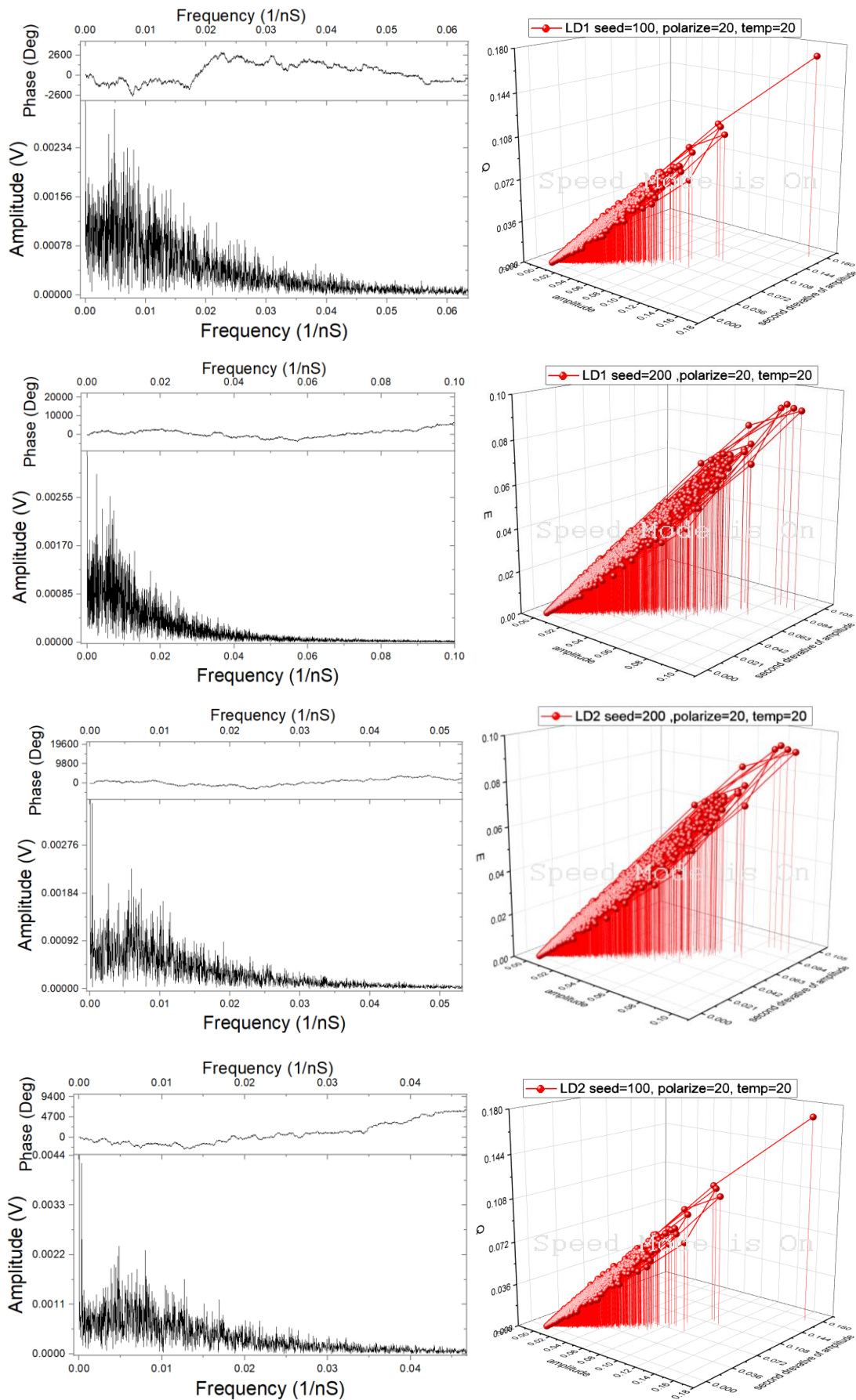


Fig. 4. Selected three dimensional chaotic attractors and their FFTs for the same measurements of time series and attractor given in Fig. 3 with: Upper row: LD1, lower row: LD2 SEED (color online)

In Fig. 4 upper row, three dimensional attractors were plotted using the origin program for best results achieved in Fig. 3. As reported by Ref. [33]; from a three-dimensional time-delay reconstructed attractor, the Poincaré section (Stokes space representation of all possible state of polarizations SOPs) can be obtained by a clock-wise rotating slicing two-dimensional plane. Attractor were denser (rout modes paths increases) with high amplitudes as we increase LD1 SEED from 100 to 200. Anomalous chaotic behavior observed only in LD1 with SEED 300, in which the oscillator be running with unique single mode, i.e. without any randomness. Consider laser devices internal interactions, theoretically, as mentioned above, SEEDs associated with Fabry-Perot etalon containing nonlinear semiconductor material with an applied electric field perpendicular to that material, with layers are quantum well confined material, optical absorption can be changed. Due to this effect, device follow bi-stability and Opto-Electronic Feedback (OEFB) if quantum confined combined with optical detection. For our technique, dynamics similar to those related with OEFB are achieved, which offers a best option in order to prevent problems associated with pure optical feedback by

simulating interplay between two primarily beams originally derived from the same light source. According this property, in reality operation, source power fluctuations results no effects into emitted signal. This will make applications that requires more stability such as cascade able logic and transmitting units, operates with higher efficiently. For the same figure, results show the same, but opposite attractors, effect that had been measured for LD1 SEED. This is due to matching virtually between laser sources LD1 and LD2 SEEDs, which interacts again.

### 3.2. Injection with FBG sensor temperature control (with variable polarization)

Fig. 5 gives the output dynamics measured from OV\_4 with variable polarization to the reflected part of injected light came from LD1 with the aid of smart FBG. As it is shown, time series are not constant, also attractors are variable according to variation of polarization for this light part and also to the applied temperature into the FBG itself.

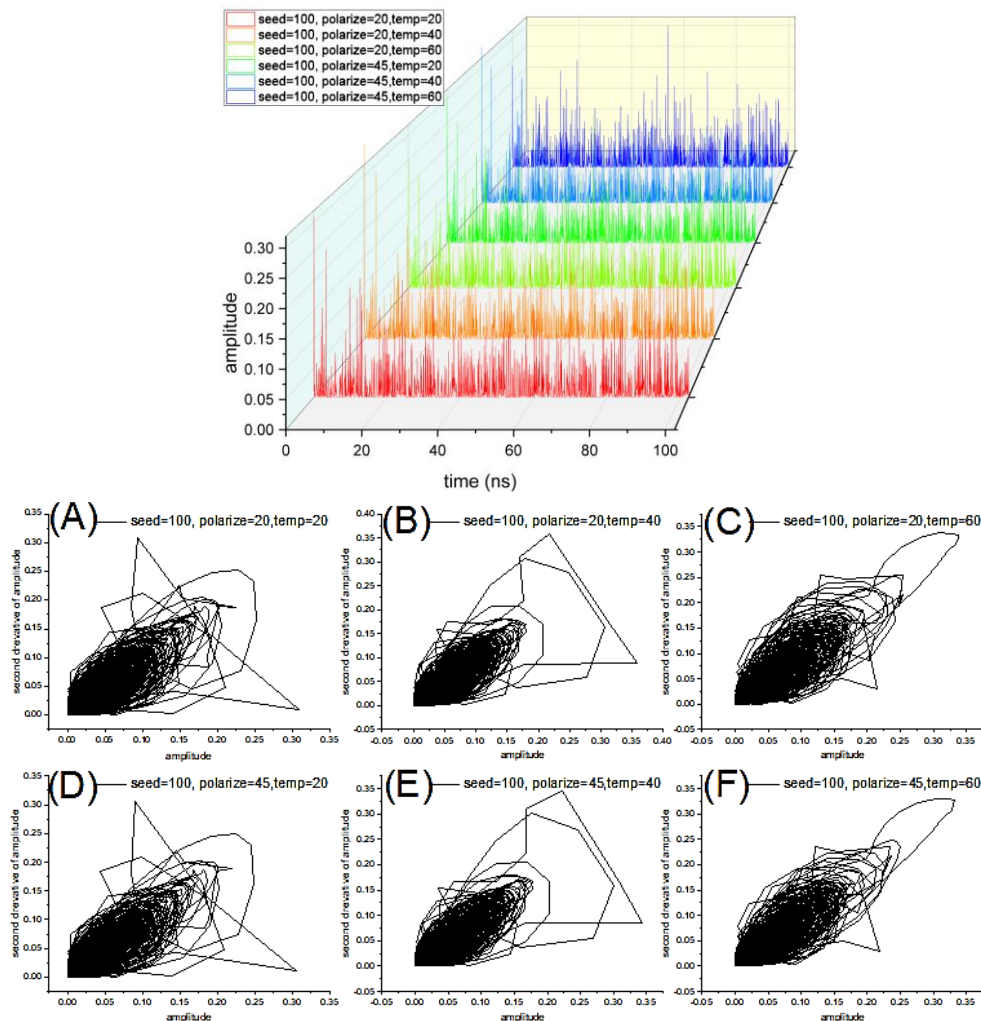


Fig. 5. Results for chaotic output measured time series from OV\_4 for signal mixing between LD1 and LD2, with constant LD1 seed (100) and LD2 seed (200), and variable both  $T$  (20, 40, 60) °C and  $P$  (20,45) degree (color online)

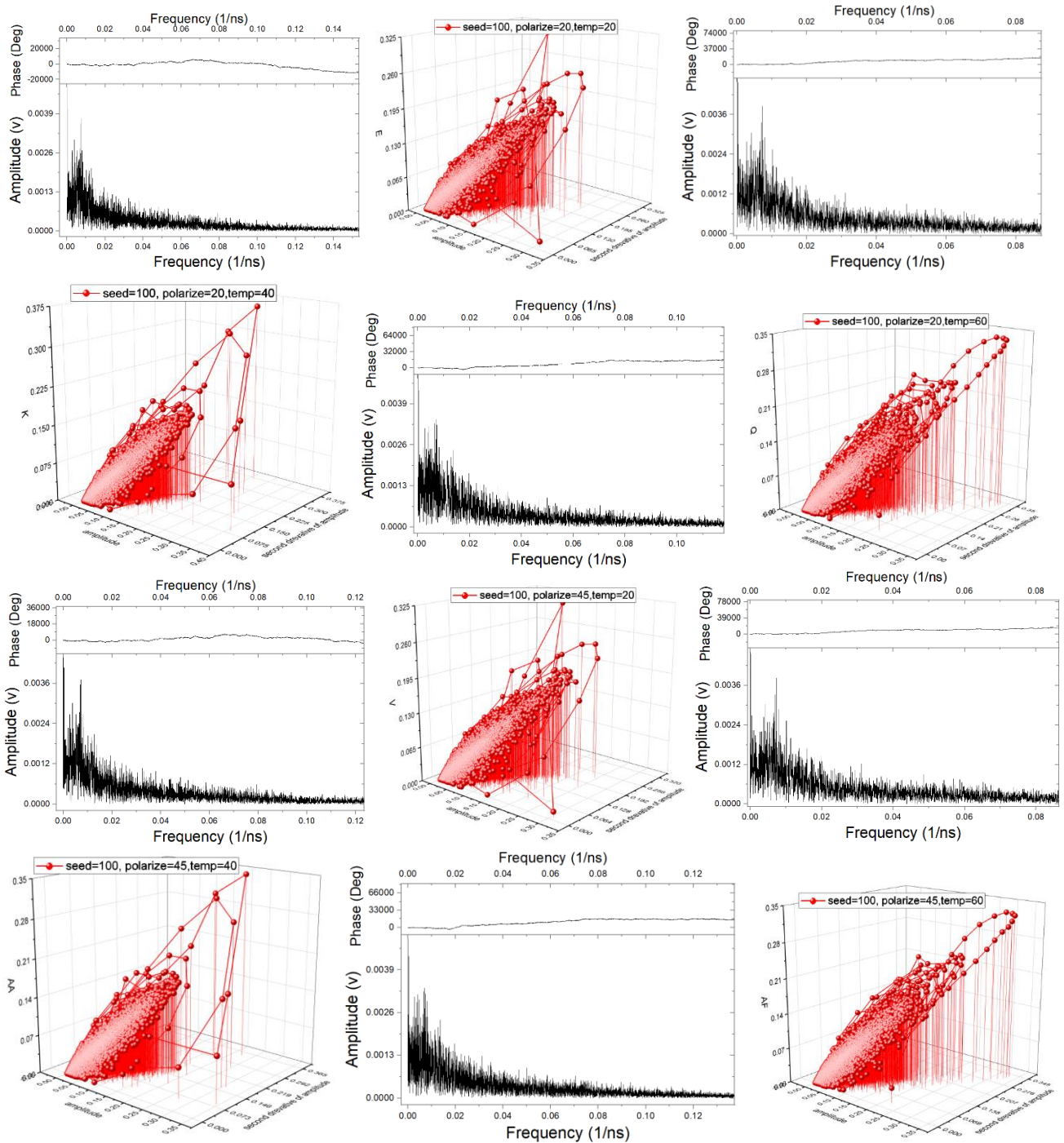


Fig. 6. Results for chaotic output mixed signal combined from LD1 and LD2 with three FBG applied temperatures (20,40,60) °C, and variable polarization. Upper row: FFTs and 3D attractors with SEED 100 and 200 for LD1 and LD2 and polarization 20. Lower row: The same SEEDs as previous part, but with polarization 45 (color online)

Polarization control is directly related with orientation of the electric field vector whose components are dependent on both the position ( $x$ ;  $y$ ;  $z$ ) and time  $t$ . For a given position  $z$  inside an optical fiber, polarization variation gives rise to randomness for the final output signal in our set up via Polarization-Mode Dispersion (PMD) that resulted by optical birefringence effect which present in optical fibers and whose evolution is random in time and space domains. Stokes parameters describe not

only the completely polarized light but also un-polarized or partially polarized light which is the expected in the first and second mixing pump probe coupler this set up. From the other hand, changing the FBG temperature can make the portion of reflected light from this FBG region linearly changes which related with PMD for this part i.e. this effect related linearly with the resulted randomness inside generated signal. According to Degree of Polarization, DOP, value un-polarized light take value of 0

and for the polarized light it takes 1. This is depending on axis for Poincaré sphere.

As shown in Fig. 6, resulted chaotic signal is affected with both polarization and FBG applied temperature. Upper row for this figure gives the results with temp variation between 20 and 60 °C, which is located within the possible ambient temperature range for silica fibers. While, increase the polarization angle to 45 gives different attractors, lower row from the same figure. Ref. [34] reported that SOP for light does not change during propagation in a homogeneous, isotropic, non-dispersed medium. Significant changes in the SOP and degree of polarization occur during propagation in an inhomogeneous medium and through optical fibers, such a controlled variation can give rise to intentionally disturbance to the overall output chaotic signal. Such a disturbance represents imperfections or external perturbations which cause mode mixing and random polarization, leading to a strong change in the polarization state in the output.

### 3.3. Injection with FBG sensor stress control (with variable polarization)

Stress-related optical fiber with birefringence that can be utilized with the FBG sensor to observe spectrum [9]. Li *et al.* predicted and experimentally demonstrated that

using a fiber Bragg grating (FBG) as a reflector can reduce the Time Delay Signature (TDS) of chaos produced from an Edge Emitting Laser (EEL) [35].

As shown in Fig. 7, the chaotic output signal is resulted from two mixing mechanisms, one of them is between the reflected and transmitted part after the second FBG region, and the second is between both signals that came from LD1 and LD2. The idea is to subjecting the FBG to several values of stress and rotating the light polarization during the operation. The stress makes an evolution for the resulted signal SOP which represent a dynamical system for increase signal security. Basically, FBG medium is a single mode fiber, which has response to outer environmental conditions by an equation consist of two terms. First term represents the contribution of strain, while the other is the temperature change or contribution. The first factor affects the reflected spectrum via force and temperature, while the second affects the glass refractive index change only due to temperature. Accordingly, our measurements were based on this idea considering both of these conditions for optimize complexity from the resulted spectrum externally or independently from laser cavity, which is the convention technique till now. For three values of stress, results are given in the following Fig. 7. Time series seems chaotically behaves, also attractors are all complicated with spectra differs than those resulted in the last section.

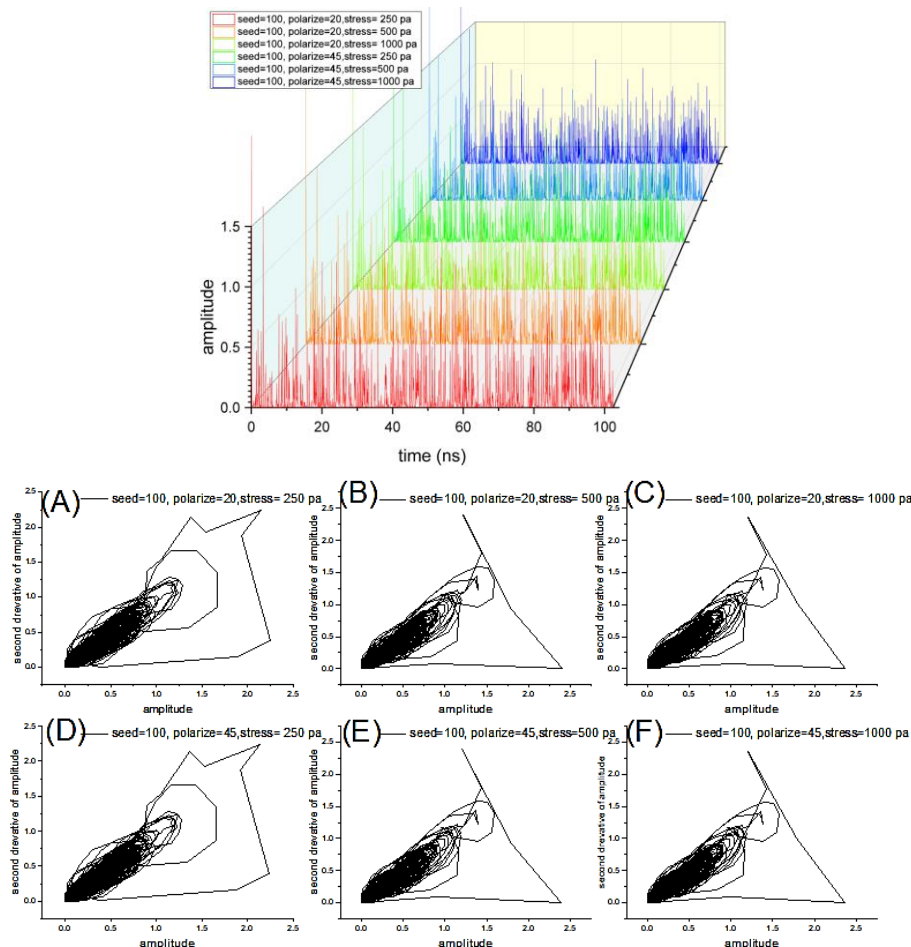


Fig. 7. Results for mixed chaotic output (OV\_4), time series and its attractors with; SEED=100, 200 for LD1 and, respectively. LD1 P is (20,45) deg, FBG sensor T (20) °C, and the applied stress changed with; (250, 500, 1000) MPa (color online)

More analysis for time tracing, i.e. FFTs, gives a wideband, nearly constant FWHM 0.04GHz frequency spectrum for all values of stress applied into the FBG, see Fig. 8.

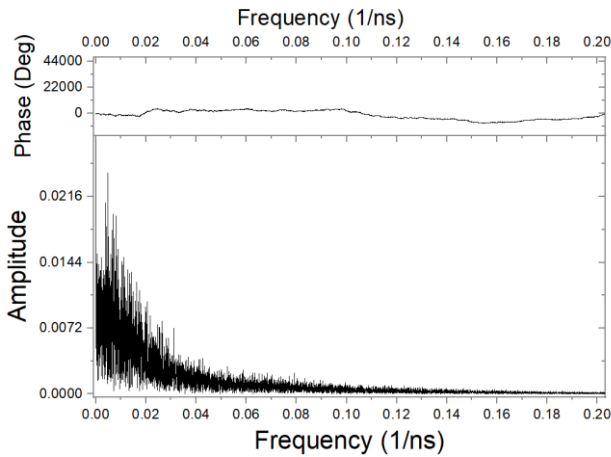


Fig. 8. FFT spectrum sample for measurements given in Fig. 7

**3.4. LD1 and LD2 cross correlation calculations**

Matching or perfect synchronization in our couple laser devices emission is avoided intentionally to increase security level for the transmitted information. Operating communication systems under tough conditions includes in reality a lot of parameter mismatch. This could lead to a drop in decryption quality with the case of complete communication system. The sensitivity of chaotic dynamics to initial conditions is also a fundamental concern. In the current work, this component is used in the opposite way, necessitating an initial mismatch between the master and slave lasers. This is to make encryption more difficult under dynamical starting conditions, which are possible due to the FBG sensor's presence.

Seed modifies the exciton absorption spectrum in a multiple quantum well, which was employed as the bistability mechanism, by causing a quantum restricted Stark effect or other quantum effects. Complex multi-stable states are affected by the power and/or wavelength of incident light entering p-i-n semiconductors. It is impossible for two bistable devices with the same spectrum to oscillate at the same moment. This makes regulating a system of oscillators at the same time desirable, especially when combined with the flexibility of a constantinuos controller to achieve complexity. Seeds can cause Hopf bifurcation and oscillation states based on input power, turning a stable LD into an unstable one [16].

Table 2. CC between LD1 and LD2 with variable SEEDs, polarization and Temp

LD1 SEED					
100		200		300	
Polarization degree					
20		45		20	
45		20		45	
Temp. °C					
20		45		20	
45		20		45	
CC					
0.320	0.324	0.331	0.318	0.321	0.324
0.337	0.336	0.317	0.332	0.334	0.310
0.108	0.123	0.124	0.108	0.132	0.123
0.132	0.123	0.108	0.124	0.132	0.123

Results for LD1 and LD2 calculated correlation for several variations including FBG T and Stress and optical injection phase are given in Tables 2 and 3. For ensure more chaotic contribution from LD1 into LD2 calculations for cross correlation is needed, accordingly, for all simulated parameters, CC is calculated and their results are given in Table 2 and Table 3. The first table is for temperature contribution and the second is for the stress. From Table 2 we conclude that although all resulted values are low enough, but still the main effect for anti-synchronization is found with LD1 when its SEED equals to 300, with polarization angle 45° and temperature 20 °C, which equals to 0.1088. This exam enhances the security level for this chaotic transmitter which make sure that each laser device contributes separately into the resulted dynamics. Fig. 9 gives the schematic diagram for this measurements.

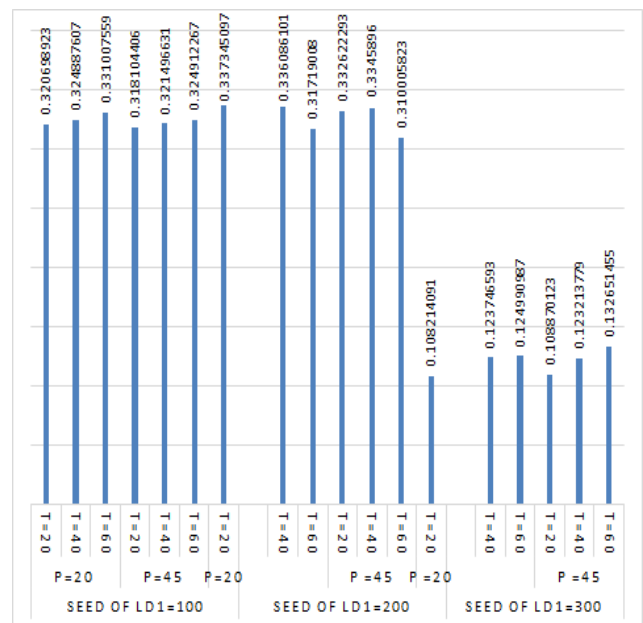


Fig. 9. CC diagram for results given in Table 1

For the same set up given in Fig. 2, the CC is also calculated for the selected parameters for determine the lowest value to ensure best anti-synchronization. As given in Table 3, lowest value is associated with stress of 500 and polarization degree 45°, with LD1 SEED 300. These results are given scheatically in Fig. 10.

Table 3. CC between LD1 and LD2 with variable SEEDs, polarization and stress

LD1 SEED value					
100		200		300	
Polarization degree					
20		45		20	
Stress KPascal					
250	500	1000	250	500	1000
0.480	0.476	0.477	0.480	0.476	0.477
0.517	0.528	0.528	0.517	0.528	0.528
0.128	0.124	0.125	0.128	0.124	0.125

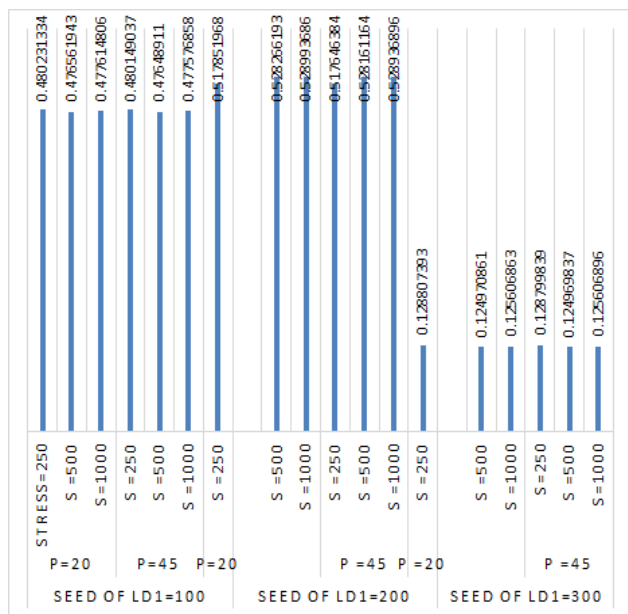


Fig. 10. CC diagram for results given in Table 1

### 4. Conclusions

Low CC and anti-synchronization between twin lasers in a chaotic transmitting unit gives an additional increase of security via unidirectional modulation from first laser. The second laser responds to fluctuations modulated upon its bias current. Besides this optoelectronic injection, laser accepts SEED as an additional perturbation source. As a result, fluctuations translate the laser from one instability level into a more complex state. A couple of smart uniform FBGs with slightly different Bragg wavelengths tune the modulated frequencies to reach the matching with

free-running relaxation oscillations by the application of either stress or variation in temperature. Laser SEED which is applied to both lasers with a different value to increase the complexity. Resulted output spectrum gives a chaotic bandwidth ranging between (0.02 to 0.06) GHz depending on polarization degree, stress, SEED and temperature.

### Acknoldgments

The authors would like to thank Mustansiriyah University, (www.uomustansiriyah.edu.iq) Baghdad – Iraq for their support in the present work.

### References

- [1] X. Mu, Z. Y. Y. Yu, H. Yan, D. Han, Optics & Laser Technology **127**, 106172 (2020).
- [2] A. A. Hemed, R. S. Abbas, AIP Conference Proceedings **2290**, 050021 (2020).
- [3] R. S. Abbas, A. A. Hemed, Journal of Physics: Conference Series, Iraqi Academics Syndicate International Conference for Pure and Applied Sciences **1818**, 1 (2021).
- [4] X. Li, W. Pan, B. Luo, D. Ma, Y. Wang, N. Li, Chaos, Solitons and Fractals **27**, 1387 (2006).
- [5] R. Vicente, J. Mulet, C. Mirasso, M. Sciamanna, Proc. of SPIE **6184**, 618413 (2006).
- [6] Gatara G. Ignace, Polarization Switching, Locking and Synchronization in VCSELs with Optical Injection, A Ph.D. Dissertation, Université Paul Verlaine Metz and the Vrije Universiteit, 2008.
- [7] M. Virte, Chaos **26**, 053108 (2016).
- [8] E. Jayaprasath, Y.-S. Hou, Z.-M. Wu, G.-Q. Xia, IEEE Access **6**, 58482 (2018).
- [9] A. A. Hamed, Studying the Effective Factors on Producing Modal Birefringence (High and Low) in the Single-Mode Optical Fiber, Baghdad: M. Sc. Thesis, Mustansiriyah University, 2005.
- [10] Z.-F. Jiang, Z.-M. Wu, W.-Y. Yang, C.-X. Hu, Y.-H. Jin, Z.-Z. Xiao, G.-Q. Xia, Chin. Phys. B **30**(5), 050504 (2021).
- [11] A. A. Hemed, T. Ackemann, H. J. Khashi, B. T. Choad, Iraqi Academics Syndicate 2nd International Conference for Pure and Applied Sciences; IOP Publishing; Journal of Physics; Conference Series, Babylon, Iraq, **1818**, 1-13 (2021).
- [12] A. H. Al-Hamdani, H. G. Rashid, Z. R. Ghayib, ARPN J. of Eng. and App. Sci. **9**(11), 2286 (2014).
- [13] Z. Sun, Z. Deng, Proceedings of 2013 Chinese Intelligent Automation Conference Intelligent Automation & Intelligent Technology and Systems, Lecture Notes in Electrical Engineering 254: Springer; 2013th edition, 243 (2013).
- [14] D. Ganziy, B. Rose, O. Bang, Applied Optics **55**(23), 6156 (2016).
- [15] Yiming Song, L. Xia, Y. Wu, IEEE Journal of

- Lightwave Technology **37**(10), 2435 (2019).
- [16] A. A. Hemed, Z. R. Ghayib, H. G. Rashid, 2nd International Conference on Physics and Applied Sciences (ICPAS 2021), College of Education, Mustansiriyah University, Baghdad, Iraq, *J. Phys.: Conf. Ser.* **1963**, 012063, 1-15 (2021).
- [17] A. A. Hemed, Chaos Generation Methods in Optical Communication Systems, Baghdad: A Ph. D. Thesis, University of Baghdad, 2011.
- [18] A. H. Mohammed, A. A. Hemed, *Journal of Kerbala University* **15**(1), 40 (2017).
- [19] P. Jiang, P. Zhou, N. Li, P. Mu, X. Li, *Optics Express* **29**(12), 17815 (2021).
- [20] J.-M. Sarraute, K. Schires, S. LaRochelle, Frederic Grillot, *IEEE Journal of Selected Topics in Quantum Electronics* **21**(6), pp.1801408 (2015).
- [21] J. Khurgin, *Applied Physics Letters* **53**(9), 779 (1988).
- [22] Y. Tadaaki, O. Yohei, K. Tomoyuki, N. Tomoyuki, N. Shigetoshi, *International Journal of Bifurcation and Chaos* **16**(12), 3717 (2006).
- [23] Nelson de Jesus Cordeiro Muga, Polarization Effects in Fiber-Optic Communication Systems, Ph. D. Thesis, Universidade de Aveiro, 2011.
- [24] A. A. Hemed, *Mustansiriyah Journal for Sciences and Education* **17**(1), 78 (2016).
- [25] B. T. C. Ayser A. Hemed, H. J. Khashi, *Mustansiriyah Journal for Sciences and Education* **16**(1), 35 (2015).
- [26] A. M. Suhail, B. T. Chead, H. J. Khashi, A. A. Hemed, *Atti Della, Fondazione Giorgio Ronchi* **65**(2), 148 (2010).
- [27] G. Millot, S. Wabnitz, *J. Opt. Soc. Am. B* **31**(11), 2754 (2014).
- [28] S. K. Ibrahim, J. A. O'Dowd, V. Bessler, J. M. Karabacak, Johannes M. Singer, *Proc. of SPIE* **10208**, 10208OP-1 (2017).
- [29] M. M. Fdhala, Effect of grating regions number on the efficiency of fiber Bragg grating sensor, M. Sc. Thesis University of Nahrain, 2020.
- [30] A. A. Hemed, M. M. Fdhala, S. M. Khorsheed, *Kuwait Journal of Science* **49**(1), 1 (2022).
- [31] A. A. Hemed, Z. R. Gaiab, 2022 International Conference on Computer Science and Software Engineering (CSASE), Duhok, Iraq, 194 (2022).
- [32] Z. R. Ghayib, A. A. Hemed, *Pramana - J. Phys.* **96**(86), 1 (2022).
- [33] Nina Sviridova, Kenshi Sakai, *Chaos, Solitons & Fractals* **7**, 53 (2015).
- [34] N. I. Petrov, *Fibers* **9**(34), 1 (2021).
- [35] Z.-Q. Zhong, Z.-M. Wu, G.-Q. Xia, *Photon. Res.* **5**(1), 6 (2017).

---

\*Corresponding author: zainabrashedgaiab@yahoo.com,  
ayser.hemed@uomustansiriyah.edu.iq